Magnetic Properties of $La_{0.67}Sr_{0.33}MnO_3$ Thin Films

Muhammad Shahbaz Anwar

محمد شہباز انور

Pre-PhD Project Report

Kamerlingh Onnes Laboratory, Leiden University,
Leiden the Netherlands

14 August 2006

The work presented in this report has been carried out in the Magnetic and Superconducting Materials (MSM) Group Kamerlingh Onnes Laboratory, Leiden University, Leiden the Netherlands, under kind supervision of Prof. Dr. Jan Aarts in collaboration of Drs. C. Beekman (Christianne).

Acknowledgments

I spent a great time in the Magnetic and Superconducting Materials (MSM) Group, Kamerlingh Onnes Laboratory, Leiden University, the Netherlands.

It is matter of great pleasure and honor for me to express my deep sense of gratitude to Prof. Dr. Jan Aarts. His pursuance guidance and encouraging attitude was real source of inspiration that helped me to complete my project well in time. I express the heartiest gratitude to Dr. Chris Bell, always having time for useful discussions. With humble profound and deep sense of devotion, I wish to record my sincere appreciation to Drs. Cristianne Beekman for her guidance and collaboration in deposition, SQUID measurements.I am also grateful to Ruud Hendrikx for XRD measurements, and helping me in Atomic/Magnetic Force Microscopy in a very nice and friendly attidute.

I have no words in my command to express my gratitude and forward admiration to my sweet and sincere research and group fellows Marcel Hesselberth, Tibi Sorop, Federica Galli, Yu-Quin Zhang, Machiel Flokstra and Simon Kelly, Jorina van der Knaap, Ismail G¨ul, Maartje Dekker, Suleyman Tursucu and Dapengh Qu.

I am also thankful to Mrs. Danielle Duijn for helping me in fulfilling the official requirements.

Muhammad Shahbaz Anwar

Dedication

To my father (late), who was always exciting me to find new things. I always remember his advice, "Look up in your educational life to give innovations and always look down in your social life to be relaxed with your position in society".

Abstract

$La_{0.67}Sr_{0.33}MnO_3$ thin films were deposited by DC sputtering deposition on various substrates. Three thin films with different thickness (20, 40,120nm) were deposited on $SrTiO_3$ substrate to investigate the dependence of magnetic microstructures on thickness of thin films. Two LSMO thin films were deposited on LAO and NGO substrates to study the effect of structural induced stress by underlying substrates on magnetic domain. It was found that magnetic microstructure has strong dependence on thickness of thin films. 20nm thick LSMO/STO thin films have featherlike magnetic domains while 40nm, 120nm thin films have straight strip like magnetic domains similar to those were seen in of 40nm LSMO thin films on LAO and NGO substrates. The magnetization was in the plane of substrate for LSMO on STO, while out of plane for LSMO on LAO. It was also analyzed that stepped substrate can induce relaxation in LSMO thin films. The ferromagnetic transition temperature was sensitive to thickness but not to type of substrate.

Contents

Chapter 1

Introduction

1.1 Introduction

The field of study of manganites thin films is revived after the discovery of high temperature superconductivity in the transition metal perovskites oxide in 1986 [1]. The perovskites manganites exhibit a variety of magnetic and electronic behaviors such as colossal magnetoresistance (CMR), gradual phase separation, spin/charge/orbit ordering and so on [2-4]. Especially the discovery of CMR effect in manganites compounds [5] has renewed the interest in this class of materials. The chemical formula of CMR manganites can be written as $RE_{1-x}A_x\ MnO_3$, where RE stands for a rare earth (mostly La Nd) and A for an alkaline earth (mostly Ca, Sr, Ba). For $0.2<x<0.5$, manganites show a number of exotic manetotransport properties related to the complete spin polarization. Substitute manganites show magnetic behavior at large temperature and show an insulating behavior at high temperature. These two regimes are separated by a metal-insulator MI transition temperature T_p. the MI critical temperature coincides fairly well with the ferromagnetic transition temperature T_c. Colossal dependence of the electric resistance on the applied magnetic field occurs in the proximity of the MI transition. The mechanisms of manetotransport in the bulk manganites have been thoroughly studied [6]. Because of their properties, manganites have attracted much interest for many possible applications, such as insulating-magnetic tunnel junction or spin valve for magnetic memories and read heads for high density data. Obviously, such applications require the utilization of manganites thin films and magnetic based heterostructures.

It has been observed that magnetic and transport properties of the manganites thin films are very sensitive to not only microstructures but also lattice induced stresses by the underlying substrate [7]. In addition the local magnetic domain structure also plays an important role in determining their properties. Kwon et al. have studied the effect of strain on magnetoresistance properties of LSMO ($La_{0.7}Sr_{0.3}MnO_3$) thin films on LAO ($LaAlO_3$) and STO (SrTiO3) substrates using Atomic Force Microscope (AFM) and Magnetic Force Microscope (MFM) [8]. Wang et al. reported that large low field magnetoresistance (MR) in PSMO ($Pr_{0.67}Sr_{0.33}MnO_3$) film on LAO in due to domain boundaries [9]. It also observed that magnetic domains

are affected by a stress induced magnetic anisotropy that is associated with lattice mismatch of the film with substrate [10-16].Wu. et al. also analyzed the MR of compressive strain on LSMO film and found evidence for a small contributed to the MR [12]. Dho. et al. investigated the effects of the anisotropic stress on magnetic domain in LSMO thin films on various substrates using MFM.

Chapter 2

Magnetic domain and domain walls

2.1 Magnetic domain

There were some interesting questions about ferromagnetic materials like, how could an applied magnetic field of few Oe fully saturate a piece of soft Fe when an internal field of a few KOe was not enough to explain the curie temperature? How did internal molecular field of the order of Moe, not fully saturate the material? The development of the Weiss molecular field, really a manifestation of exchange interaction was part of the answer, but the other part was to suppose that the sample was made up of various fully magnetized regions, called magnetic domains [17].

2.2 Domain Wall

Domain wall is a topological defect in the magnetically ordered state of a solid. The idea of the magnetic domains was first postulated by Weiss [18] although the term domain was not introduced until much later [19]. The idea about magnetic domains was reviewed by Kittle [20].

The physical principle of minimizing magnetostatic energy which is responsible for formation of domain wall was forwarded by Landau-Lifschitz in 1935 [21] along with famous Landau-Lifschitz wall profiled,

$$\theta \propto \tanh(\frac{x}{D})$$

Where, x is the position coordinate and D is the wall thickness parameter. It is the modified form of Bloch's proposal [22]. Basically, domain formation is the competition between the various energy terms those describe a magnetic object:

- Exchange Energy
- Anisotropy Energy
- Zeeman Energy
- Magnetostatic Energy

2.3 Exchange energy

The Heisenberg Hamiltonian of the exchange interaction is usually written in the form

$$H_{exch} = -\sum_{i,j=i}^{M} J_{ij} S_i . S_j$$

Where, J_{ij} is the exchange integral, which can be calculated using quantum mechanics [23-24]. It decreases rapidly with increasing distance between the atoms, and so the sum has to be taken only for nearest neighbours and we can write J for $J_{ij}.S_{ij}$ stands for the spin operators. If we replace them by classical vectors and rewrite the dot product, we obtain relation for the exchange energy,

$$E_{exch} = -JS^2 \sum_{i,j|i\neq j} \cos\varphi_{ij}$$

By making the use of small angle approximation for φ_{ij}, Taylor series expansion for cosine, take the sum for each pair of nearest neighbours only once and redefine the zero level of the exchange energy by removing the constant term. Relation () can be written under above considerations as

$$E_{exch} = -JS^2 \sum_{NN} \varphi_{ij}^2$$

For small angles φ_{ij} can be written as,

$$\varphi_{ij} \approx \left|(r_i.\nabla)m\right|$$

Where, r_i is the position vector from site i to j and m is the continuous variable for the magnetization. Then, the exchange energy is given by

$$E_{exch} = JS^2 \sum_{i} \sum_{r_i} \left|(r_i.\nabla)m\right|^2$$

Changing the summation over i to an integral over the ferromagnetic body,

$$E_{exch} = A[(\nabla m_x)^2 + (\nabla m_y)^2 + (\nabla m_z)^2]\, d^3 r$$

2.4 Magnetocrystalline anisotropy energy

The Heisenberg Hamiltonian is completely isotropic, and its energy levels do not depend on the direction in space in which the crystal is magnetized. If there was no other energy term, the magnetization would always vanish in zero applied field. However, real magnetic materials are not isotropic. So the permanent magnets in microphones and loudspeakers do not lose their permanent magnetization after production.

The most common type of anisotropy is the Magnetocrystalline anisotropy, which is caused by the spin-orbit interaction of the electrons. The electron orbits are linked to the crystallographic structure, and by their interaction with the spins they make the latter prefer to align along well-defined crystallographic axes. Therefore, there are directions in space, in which a magnetic material is easier to magnetize than in others. The axis along which magnetization is easy to align is called easy axis and other is called hard axis. The spin-orbit interaction can also be evaluated from basic principles. However, it is easier to use phenomenological expressions (power series expansions that take into account the crystal symmetry) and take the coefficients from experiment. The magnetocrystalline energy is usually small compared to the exchange energy. But the direction of the magnetization is determined only by the anisotropy, because the exchange interaction just tries to align the magnetic moments parallel, no matter in which direction. In hexagonal crystals the anisotropy energy is a function of only one parameter, that is the angle between the magnetization and the c-axis. Experiments show, that it is symmetric with respect to the base plane, and so odd powers of $\cos\theta$ can be omitted in a power series expansion for the anisotropy energy density E_{ani}. The first two terms are thus,

$$E_{ani} = -K_1 \cos^2\theta + K_2 \cos^4\theta = -K_1 m_z^2 + K_2 m_z^2$$

Where z is parallel to the c-axis. It is known from experiment, that terms of higher order and in most cases even K_2 are negligible. If $K_1 > 0$, then the c-axis is an easy axis, which means it is a direction of minimal energy. For $K_1 < 0$ it is a hard axis with an easy plane perpendicular to it.

2.5 Magnetostatic energy

The origin of domains still cannot be explained by the two energy terms above. Another contribution comes from the magnetostatic self-energy, which originates from the classical interactions between magnetic dipoles. For a continuous material it is described by Maxwell's equations

In our magnetostatic problem, we do not have any electric fields E or free currents j. Thus, there are two remaining equations

$$divB = 0$$
$$curlH = 0$$

The magnetic induction B is given by $B = \mu_o(H + M)$. A general solution for is given by

$$H = -\nabla U$$

Where U is the magnetic scalar potential. Using the expressions for B and H we get,

$$\Delta U_{in} = divM$$

Inside magnetic bodies and

$$\Delta U_{out} = 0$$

Outside in air or vacuum.

These equations have to be solved with the boundary conditions

$$U_{in} = U_{out} \qquad \frac{\partial U_{in}}{\partial n} - \frac{\partial U_{out}}{\partial n} = M.n$$

On the surface of the magnet to obtain $\underline{U}$ and derive from it H. n is the unit normal to the magnetic body, taken to be positive in outward direction.

Finally the magnetostatic energy is given by

$$E_{ext} = -\frac{1}{2}\mu_o \int_v M.H_{ms} d^3 r$$

Where, H_{ms} is the demagnetizing field.

2.6 Zeeman energy

For the energy of a magnetic body in an external field H_{ext} we obtain

$$E_{ext} = -\mu_o \int_v M.H_{ext} d^3 r$$

Due to the linearity of Maxwell's equations, the superposition principle allows a simple adding also of this energy term.

The total energy is simply a sum of these terms,

$$E = E_{exch} + E_{ani} + E_{zeeman} + E_{mag}$$

The magnetic system seeks to minimize its overall free energy. As the magnitude of magnetization vector is fixed so there is the only way to do so is to vary its direction that leads to formation of domain walls. The first three of these energy terms align the spins, with each other (E_{exch}), with an easy axes (E_{anis}), with the applied external magnetic field (E_{zeeman}).some comparison may be found among these to determine to overall lowest energy direction for the magnetization. Minimizing these terms alone would

not give rise to any non-uniformity in the magnetization as this will mean that some spins will no longer be pointing along this optimal direction.

It is the magnetostatic dipole-dipole interaction that gives rise to the formation of domain structure any uniformly magnetized body will have lines of M that terminate on its surfaces. These sources and sinks of lines of magnetization will give rise to a nonzero divergence at these points. Using the basic relation $B = \mu_o(H + M)$ divergence of M can be expressed as,

$$\nabla.M = \frac{\nabla.B}{\mu_o} - \nabla.H$$

According to Maxwell equation $\nabla.B = 0$, above equation would be,

$$\nabla.H = -\nabla.M$$

Hence these sources and sinks of magnetization at the sample surfaces will give rise to a field H that ensures the continuity of lines of B. this field is known as the demagnetizing field, as it acts to educed the B inside the material to be less than the $\mu_o M$ that might be expected at zero applied field.

The energy associated with this stray field H is expressed in the form of two equivalent integrals,

$$E_m = \frac{1}{2}\mu_o \int_{allspace} H^2 dV = -\frac{1}{2}\mu_o \int_{sample} H.MdV$$

Notice that the first of these two expressions is always positive as it contains H^2 the second must also is positive as they are equal. The system would try to minimize this energy term as much as possible of course, and so in practice this means making the stray field as small as possible, as stray field energy can never be less than zero. The second integral is physically more transparent. The integrand can be seen to express the energy of a dipole MdV in the field created by all the others. The factor of $1/2$ is there to avoid double counting over the dipole. By forming non-uniform, flux closed magnetic states it is possible to reduce the number of lines of M that terminate on the sample surfaces and hence reduce the magnetostatic energy.

The formation of domains therefore proceeds until the fall in magnetostatic energy is balanced by the exchange and anisotropy energy costs associated with the twists and deviations in magnetic structure. The Zeeman energy will also play a role if a field is applied. This field may be large enough to erase the domain state and produce a uniform, magnetically saturated state again.

2.7 Types of Domain Walls

A domain is a region of uniform magnetization, which is generally separated from neighbouring domains by a domain wall that has essentially a finite thickness. Domain walls of many types are possible, but here in the figure (1) only the two simplest types: the Block wall and the Neel wall are illustrated. Furthermore, domain walls are classified by the difference in the orientations of the domains that they separate, expressed in degrees.

In the figure (1) it is supposed that the center of the domain wall at x = 0, domain is magnetized in the Y-axis. As one goes from one domain to the other, if the magnetization rotates about the X-axis, it remains in the plane of the wall, and the wall is said to be a Block wall. On the other hand, if the magnetization rotates about the z axis, the wall is said to be a Neel wall.

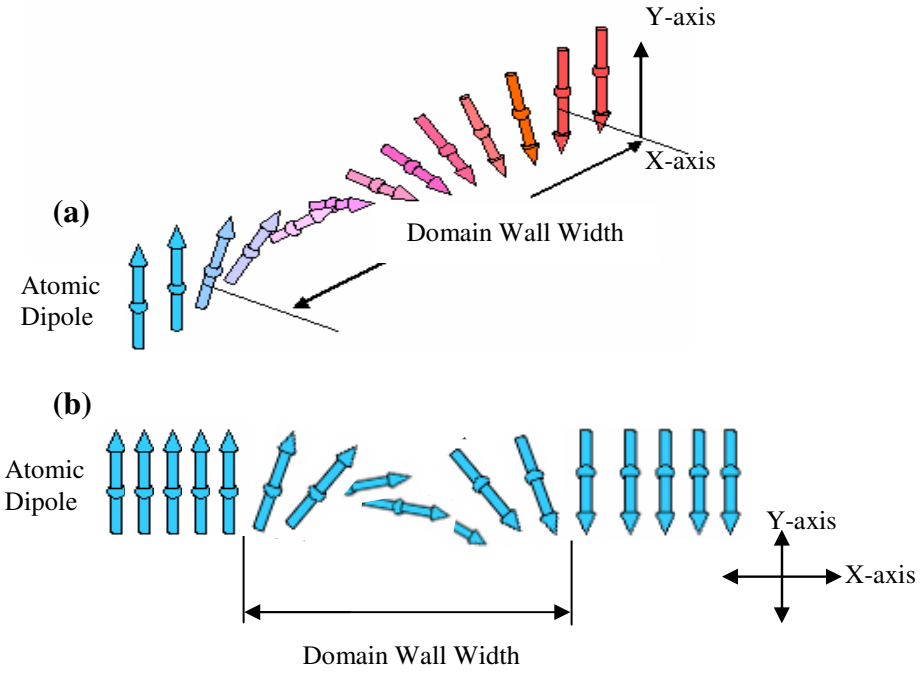

Figure 2.1: movement of atomic dipole inside a the domain wall (a) the rotation of the moment defines a Block Wall (b) in Neel's Wall moments rotate in the plane.

2.8 Domain wall thickness and energy

Suppose that we have two semi-infinite domains separated by a wall which is N planes of spins thick and the distance between neighbouring planes is lattice constant a. the magnetization rotate by 180 degree

from one domain to the next. We assume that we have uniaxial anisotropy, each domain each domain occupies one of the easy axes. Supposition is a Bloch wall for simplicity as shown in the figure (1-a).
The exchange energy associated with a pair of neighbouring spins S1 and S2 is,

$$-2JS_1.S_2 = -2JS^2\cos\varphi$$

Where φ is the angle between them and J is the exchange integral. As the exchange is very strong on short length scales, so the angle φ between one spin and the next can only ever be small. Thus above formula can be written as,

$$JS^2\varphi^2 + const.$$

This is analogous to an elastic energy, with φ taking the place of a strain. In physics one can often define such a generalized elasticity and the theory of spin waves can be recast in the form of deformations of an elastic medium with the exchange providing the restoring force. Therefore exchange stiffness can be defined as,

$$A = \frac{n}{a}JS^2$$

Where n is the number of atoms per unit cell. Let us suppose that $n = 1$, for a simple cubic lattice.
In this supposed domain wall the magnetization rotates over N planes of spins. There will be $1/a^2$ atoms per unit area in each plane, so the number of spines per unite are of wall will be N/a^2. The angle φ between neighbouring planes must be π/N. Using these all relation the exchange energy per unite area will be,

$$E_{ex} = \frac{N}{a_2}JS^2\varphi^2 = \frac{N}{a_2}JS^2(\frac{\pi}{N})^2 = \frac{A\pi^2}{aN}$$

Above equation indicates that $E_{ex} \propto 1/N$, so exchange wants to make N as large as possible thus rotation is as gradual as can be. The exchange energy will attempt spread the wall out to be infinity thick.
However, the domains occupy easy axis orientations so that within the wall the spins are in a hard direction. This costs energy of order the anisotropy constant K per unit volume of wall. This leads to energy per unit area of the wall due to anisotropy that is given by,

$$E_{an} = K(\frac{N}{a^2})a^3 = KNa$$

In this expression $E_{an} \propto N$ so anisotropy wants to compress the wall as thin as possible in order to keep all the spins in easy direction.

The total wall energy per unit area is going to be the sum of these two energy terms,

$$\sigma_{wall} = E_{ex} + E_{an} = \frac{A\pi^2}{aN} + KNa$$

The equilibrium wall will find a value for N where E_{wall} is a minimum,

$$\frac{\partial E_{wall}}{\partial N} = -\frac{A\pi^2}{aN^2} + Ka = 0$$

Solving this expression for N we get,

$$N = \frac{\pi}{a}\sqrt{\frac{A}{K}}$$

The wall thickness will be,

$$D = Na = \pi\sqrt{\frac{A}{K}}$$

By putting these values in above equation for wall energy per unit area, we get,

$$\sigma_{wall} = 2\pi\sqrt{AK}$$

This is the cost of the creation of the unit area of the domain wall in terms of exchange and anisotropy contributions only. Whether or not the wall forms, and the type of the wall if it does, will be determined by comparing this to the possible reduction in magnetostatic energy as the wall energy is proportional to the area of the wall, there is something like a surface tension that will tend to make walls appear as flat sheets so far as is possible.

It is interesting to note that the magnetostatic term, which gives rise to the domains and hence walls between them, does not really have anything to do with setting the spatial scale or energy cost of forming these walls. This is done by the exchange and anisotropy. Exchange is short ranged interaction, in above calculations exchange interaction was used only between nearest neighbours in the lattice. Anisotropy is completely local in this model, closely mirroring reality; this is the case for materials exhibiting so-called single ion anisotropy, whilst only nearest neighbours are important in those showing double ion anisotropy.

Chapter 3

Experimentation

3.1 Introduction

For deposition of perovskites thin films such as High temperature superconductors and manganites, pulsed laser deposition and DC sputtering deposition techniques are being used extensively. In this project DC sputtering deposition technique was used to deposition thin films of LSMO on different substrates and of different thicknesses as well. This chapter describes the different experimental techniques which were utilized in deposition and characterization of above mentioned thin films.

3.2 DC Sputtering Deposition

In dc sputtering deposition of oxide thin films, oxygen gas is used as an ambient gas inside the chamber during deposition. A potential difference is applied a negatively charged cathode and grounded chamber. The negatively charged cathode also contains target material. A dc discharge is produced owing to applying a high dc voltage. This dc discharge is responsible for production of ionization of processing gas. So, ions of gas are accelerated toward the cathode which contains target material, and bombarded it, thereby target material is sputtered out through collisional sputtering.

Target-to-substrate distance, substrate temperature and ambient gas pressure are crucial parameters for the uniformity, growth quality and deposition rate. But in case of DC sputtering deposition the processing gas pressure is more important parameter. Because rate of deposition is very sensitive to this parameter. At low pressures, the ionization takes place far from the target so; the probability of reaching the ions on the surface of target is reduced. Meanwhile due to the long mean free path electrons disappear at the anode. This leads to low ionization rate of gas and low deposition rate as well. With increasing of gas pressure the mean free path of electrons decreases but ionization efficiency increases, so that sputtering current and deposition rate goes up.

At too high pressures, the interaction between sputtered atoms and gas atoms or molecules scatters the sputtered target atoms away from the substrate. Therefore deposition rate decreases. Thus deposition rate

shows a peak as a function of ambient gas pressure. In general deposition rate is proportional to the sputtering power and inversely proportional to target-to-substrate deposition.

In this project all thin films are deposited in an on-axis DC oxide sputtering deposition system, details can be found elsewhere [25]. As the target material $La_{0.67}Sr_{0.33}MnO_3$ so substrate were also selected form perovskites family with lattice mismatch, to see the effect of strains on magnetic properties of thin films of LSMO. Fir this purpose (100) $SrTiO_3$ (STO) and (100) $LaAlO_3$ (LAO) were used with miscut less that 0.1°. One STO substrate with 2° miscut was also used to study the relational related to miscut in thin films.

All thin films were deposited at 3mbar oxygen pressure, 350 mA sputtering current and almost 400V potential difference. The substrate was kept at 840 C°.

3.3 Measurements for lattice parameters and thickness of thin films

X-ray Diffraction experiments are performed utilizing a Siemens D5005 X-ray vertical diffractometer (Cu-Kα) generally it carries out a θ-2θ scan, which involves the coupling of rotation of source and detector in a 1:2. During θ-2θ scan the position of X-ray beam remains fixed on the surface of the sample. The working of XRD is illustrated in the figure (2.1).

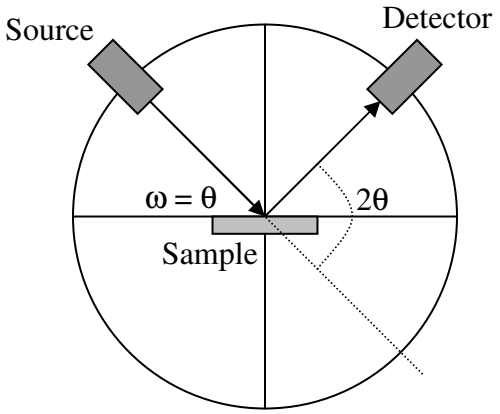

Figure 3.1: Schematic illustration of X-ray Diffractometer.

As the angles of incidence and reflection are same thus only the planes are detected, which are parallel to the surface of the sample. Using X-ray diffraction both in plane and out of plane lattice parameters can be

determined. Because of epitaxial cube on cube growth, (00*l*) type peaks of the thin films are along the normal of the substrate. Thus such peaks are used to measure the out of plane lattice parameters. In figure (3.2) peaks are shown of θ-2θ scan, for SRO substrate and LSMO thin film on it with 20nm thickness.

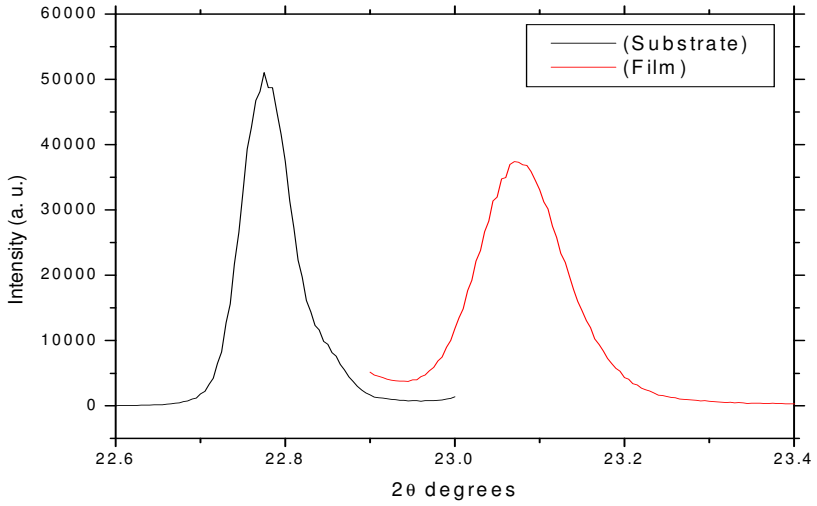

Figure 3.2: θ-2θ scan of (001) peak of 40nm $La_{0.67}Sr_{0.33}MnO_3$ thin film on $SrTiO_3$ substrate.

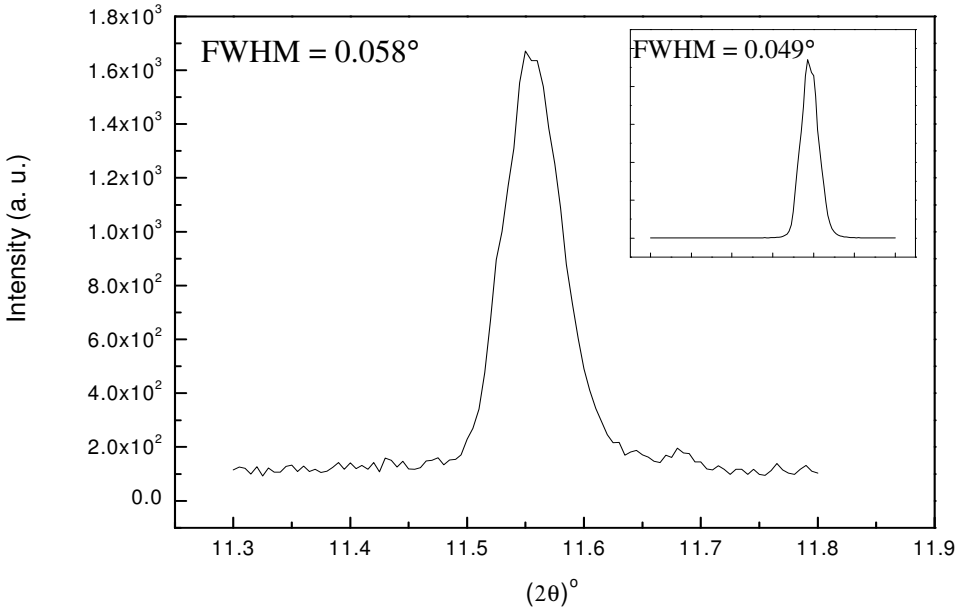

Figure 3.3: Rocking Curve of (001) peak of the 20nm $La_{0.67}Sr_{0.33}MnO_3$ deposited on $SrTiO_3$ at 840°C. The inset shows the rocking curve of the substrate

Rocking curve measurements made by doing a θ scan at a fixed 2θ angle, the width of which is inversely proportionally to the dislocation density in the film and is therefore used as a gauge of the quality of the film. Sharper the rocking curve (i.e. smaller FWHM), higher the crystalline perfection. As an example, figure (3.3) shows a rocking curve for (001) of a 20nm LSMO thin film deposited on STO substrate.

The thickness of the thin films was measured by X-ray reflectometry (XRR). XRR involves measuring the reflection of the X-ray beam from sample at grazing angles. A monochromatic X-ray beam of wavelength 15.4nm is used. Figure (3.4) shows an example of measurement of thickness of 20nm LSMO thin film.

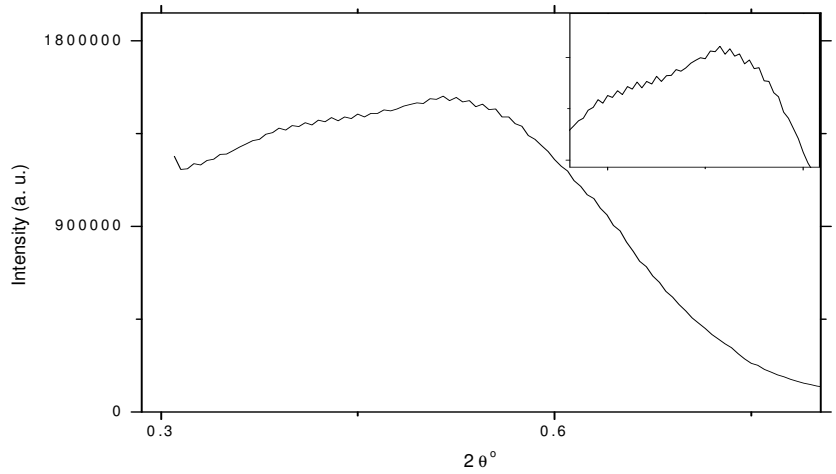

Figure 3.4: Intensity profile of 20nm $La_{0.67}Sr_{0.33}MnO_3$ thin film on $SrTiO_3$. Thickness of thin film is calculated by measure of period of variation in intensity with respect to angle. These variations are produced due to interference in reflected beams from interface of film and substrate. The inset is an enlarge of the oscillatory part.

3.4 Atomic Force Microscopy

The atomic force microscope (AFM) or scanning force microscope (SFM) was invented in 1986 by Binnig, Quate and Gerber. Like all other scanning probe microscopes, the AFM utilizes a sharp probe moving over the surface of a sample in a raster scan. In the case of the AFM, the probe is a tip on the end of a cantilever which

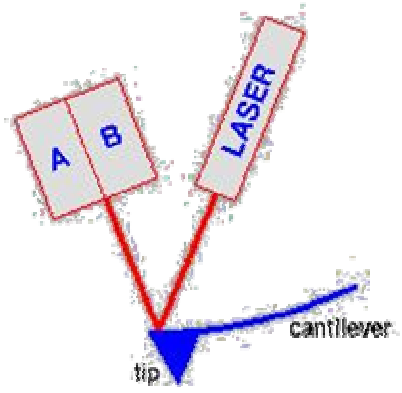

Figure 3.5: Working Principle of Atomic Force Microscope's tip

bends in response to the force between the tip and the sample.

The first AFM used a scanning tunneling microscope at the end of the cantilever to detect the bending of the lever, but now most AFMs employ an optical lever technique. The cantilever flexes, the light from the laser is reflected onto the split photo-diode as shown in the figure (3.5). By measuring the difference signal (A-B), changes in the bending of the cantilever can be measured.

Since the Cantilever obeys Hooke's Law for small displacements, the interaction force between the tip and the sample can be found. The movement of the tip or sample is performed by an extremely precise positioning device made from piezo-electric ceramics, most often in the form of a tube scanner. The scanner is capable of sub-angstrom resolution in x-, y- and z-directions. The z-axis is conventionally perpendicular to the sample.

The way in which image contrast is obtained can be achieved in many ways. The three main classes of interaction are ***contact mode***, ***tapping mode*** **and** ***non-contact mode***.

3.4.1 Contact mode

It is the most common method of operation of the AFM. As the name suggests, the tip and sample remain in close contact as the scanning proceeds.

One of the drawbacks of remaining in contact with the sample is that there exist large lateral forces on the sample as the drip is "dragged" over the specimen.

3.4.2 Tapping mode

Tapping mode is the next most common mode used in AFM. When operated in air or other gases, the cantilever is oscillated at its resonant frequency (often hundreds of kilohertz) and positioned above the surface so that it only taps the surface for a very small fraction of its oscillation period. This is still contact with the sample in the sense defined earlier, but the very short time over which this contact occurs means that lateral forces are dramatically reduced as the tip scans over the surface. When imaging poorly immobilised or soft samples, tapping mode may be a far better choice than contact mode for imaging.

Other (more interesting) methods of obtaining image contrast are also possible with tapping mode. In constant force mode, the feedback loop adjusts so that the amplitude of the cantilever oscillation remains (nearly) constant. An image can be formed from this amplitude signal, as there will be small variations in this oscillation amplitude due to the control electronics not responding instantaneously to changes on the specimen surface.

More recently, there has been much interest in phase imaging. This works by measuring the phase difference between the oscillations of the cantilever driving piezo and the detected oscillations. It is thought that image contrast is derived from image properties such as stiffness and viscoelasticiy. Digital Instruments has an application note on this topic.

3.4.3 Non-Contact Mode

Non-contact operation is another method which may be employed when imaging by AFM. The cantilever must be oscillated above the surface of the sample at such a distance that we are no longer in the repulsive regime of the inter-molecular force curve. This is a very difficult mode to operate in ambient conditions with the AFM. The thin layer of water contamination which exists on the surface on the sample will invariably form a small capillary bridge between the tip and the sample and cause the tip to "jump-to-contact".

Even under liquids and in vacuum, jump-to-contact is extremely likely, and imaging is most probably occurring using tapping mode.

A different geometry is possible using the shear-force microscope (SHFM), and here true non-contact operation is possible.

3.4.4 Lift mode

Several techniques in AFM rely on removing topographical information from some other signal. Magnetic force imaging and Electrostatic force imaging work by first determining the topography along a scan line, and then lifting a pre-determined distance above the surface to re-trace the line following the contour of the surface.

In this way, the tip-sample distance should be unaffected by topography, and an image can be built up by recording changes which occur due to longer range force interactions, such as magnetic forces.

3.5 Magnetic Force Microscopy

Magnetic force microscopy (MFM) images the gradient of magnetic forces on a sample surface. For MFM, the tip is coated with a ferromagnetic thin film such as cobalt with downward magnetization vector. The system operates in non-contact mode, detecting changes in the resonant frequency of the

cantilever induced by the magnetic field's dependence on tip-to-sample separation as shown in the Figure (3.6).

An image taken with a magnetic tip contains information about both the topography and the magnetic properties of a surface. The quality and type of the image depend upon the distance of the tip from the surface. If the tip is close to the surface, in the region where standard non-contact AFM is operated, the image will be predominantly topographic. As you increase the separation between the tip and the sample, magnetic effects become apparent. Because the interatomic magnetic force persists for greater tip-to-sample separations than the van der Waals force. In first scan tip collects the topography while in second it lifts up and collect the magnetic image.

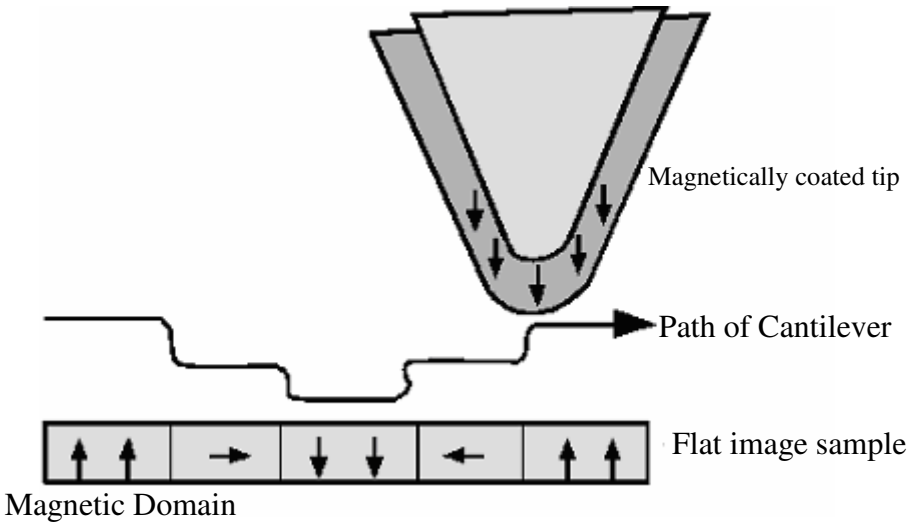

Figure 3.6: MFM maps the magnetic domains of the sample surface.

For detecting domains on oxide thin films it should be noted that the distance of the tip should larger but drive amplitude should be smaller.

3.6 Measurements of magnetic properties

Magnetic properties of LSMO thin films on various substrates, such as magnetic loops, coercivity, saturation magnetization and magnetization vs. temperature were measured in a commercial SQUID magnetometer (quantum design) with a magnetic field of 5T and a range of temperature from 30 to 400K. The roughness and surface morphology of LSMO thin films were studied using AFM, while magnetic domains were analyzed by MFM. MFM was utilized with out any applied magnetic field.

Chapter 4

Results and Discussions

$La_{0.67}Sr_{0.33}MnO_3$ thin films exhibit giant and even colossal magneto resistance. LSMO thin films could find the utilizations in next generation of magnetic sensors, potential applications in computer information storage and the automobile industry. These suggested applications renew the study of thin films of CMR materials. The objective of the project was to investigate the effect of structural strains induced by substrates on magnetic microstructures of LSMO thin films and dependence of thickness on magnetic domains in case of LSMO/STO thin films as well. For this propose LSMO thin films were deposited on (100) STO, (100) LAO and NGO substrates. To analyze thickness dependence, three thin films were deposited on STO with 20, 40, 120 nm and 25nm (on 2degree stepped substrate) thickness.

The c-axis lattice constants of LSMO thin films (40nm) on STO and LAO calculated from XRD (given in table 4.1) are 3.8539 (mismatch = 0.0666 & Distortion = 1.0127) and 3.9491 (mismatch = -1.1663 & Distortion = 0.9708) respectively. This reveals that STO exerts tensile stress while LAO compressive stress on LSMO thin films. The difference in stain induced by underlying substrates produced drastic changes in magnetic microstructures of the LSMO thin films.

To study the surface morphology of LSMO thin films we utilized AFM. The micrographs of AFM indicate the shape and size of grains dependent on substrates. LSMO on STO (20nm) (see figure 4.1-4.3) and on NGO (40nm) (see figure 4.5-b) have big grains of about round shape which were mixed to each other. Uniform thin films are observed on STO (120nm) followed by elongated grains. While grains with higher concentration and like sharp islands are dominant on LAO due to compressive stress as shown in figure (4.5-a). It is also investigated that thin films are more uniform on stepped substrate (see figure 4.4). The root mean square roughness values of LSMO thin films on STO 0.87 (20nm), 2.5966 (25nm 2° stepped), on LAO 1.2828, on NGO 0.79191.

Figure (4.6) shows the magnetization versus temperature curves for LSMO thin films on STO, LAO and NGO, gives evidence that the ferromagnetic transition temperature is 321K, 336K, and 316K respectively for 40nm thin films. It also clear that LSMO on STO with 120 nm thickness has Curie temperature (T_c) about 341K. All values are given in table 2. Hence LSMO on STO, LAO, and NGO have same T_c that is abour 320K. So Tc is independent of substrate but dependent on thickness of thin film.

Magnetization versus applied magnetic field curves for LSMO on STO and LAO are shown in the figure (4.7) at 30K temperature. These measurements provide evidence that LSMO on STO has in plane magnetization that is effect of tensile stress, while LSMO on STO has out of plane magnetization owing to compressive stress. The values of Coercive fields are given in the table 2. To analyze the magnetic loop *($M(H_a)$)* for LSMO on NGO is very difficult because of huge signal from NGO substrate. Thus it is easy to see magnetic domains on LSMO thin films on LAO but difficult in case STO due to in plane magnetization.

To analyze the effect of thickness on micromagnetic structure (magnetic domains) of LSMO thin films on STO, four films 20nm, 40nm, 120nm and 25nm on 2 degree stepped STO were deposited. MFM was utilized at room temperature and zero applied magnetic field. Feather like weak magnetic domains were observed on 20nm thin films as shown in the figure (4.8). As magnetization vector of LSMO thin films on STO is along the plane of the substrate (see figure 4.7), which is difficult to analyze by MFM. But presence of the Block wall can produce magnetic contrast. So, LSMO on STO 20nm have the Block wall as well as Neel walls, which produced feather like magnetic domains. The magnetic domain became clear by increasing the thickness of the thin films (as shown in the figures 4.9 & 4.10). Basically, increase in the thickness produced the relaxation in the thin films.

Magnetic domain structure is clearer of LSMO on 2° stepped STO substrate with 25nm thickness as compared to 40nm LSMO/STO (see figure 4.11). It is clear that steps provide the relaxation that is responsible for clear magnetic microstructures on STO substrates.

Strip like magnetic domains were observed on LSOM thin films on LAO (figure 4.12) and NGO (figure 4.13) thickness of both thin films is 40nm. Same structure was also developed on LSMO/STO with 120 nm thick thin films almost of same spacing in every case. Hence magnetic microstructures of LSMO are dependent on substrate induced strain and thickness of film as well.

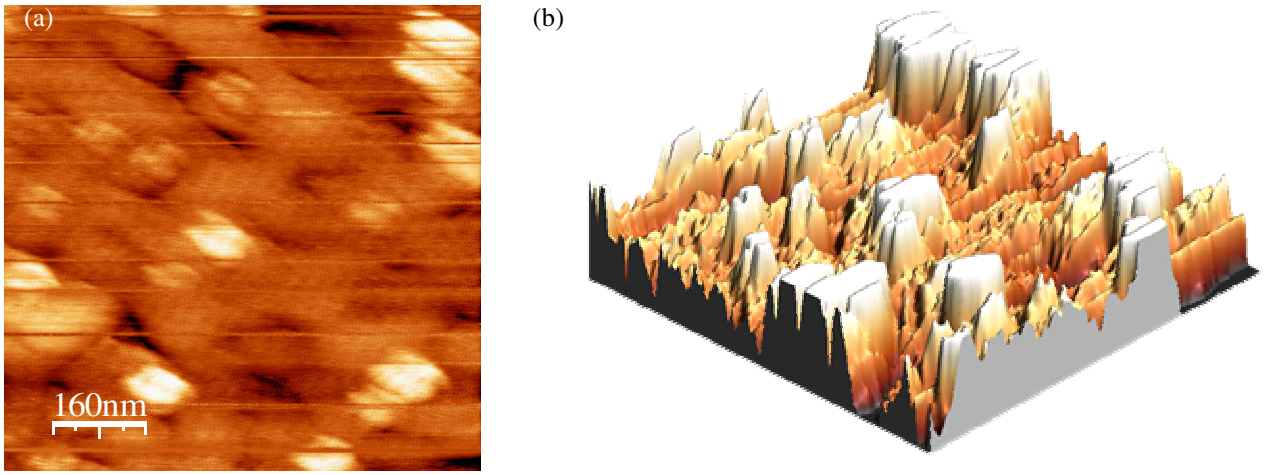

Figure 4.1: AFM micrograph (796.7nm×796.7nm) of LSMO/STO (x=0.33) thin film (20nm) (a) indicated the presence of grains on the film surface. It is also clear that most of them are flat grains. The film was deposited 840°C. (b) 3D micrograph.

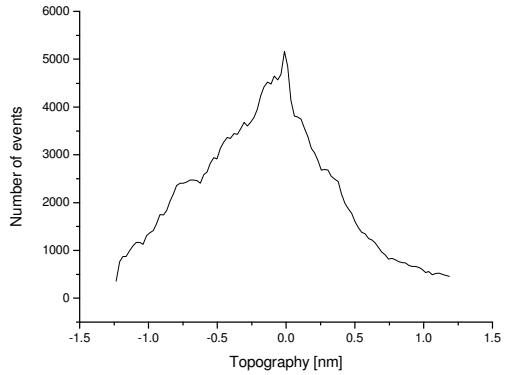

Figure 4.2: Roughness analysis of LSMO/STO, which indicates the average roughness, is

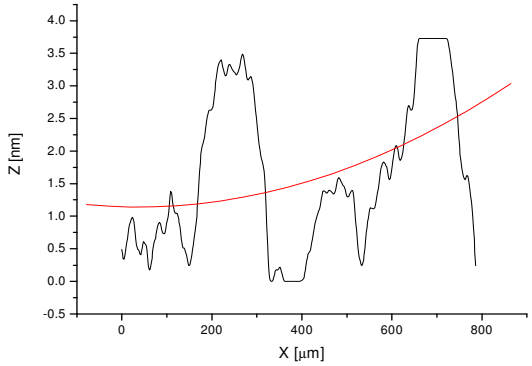

Figure 4.3: Thickness Profile of AFM Image from left top to right bottom

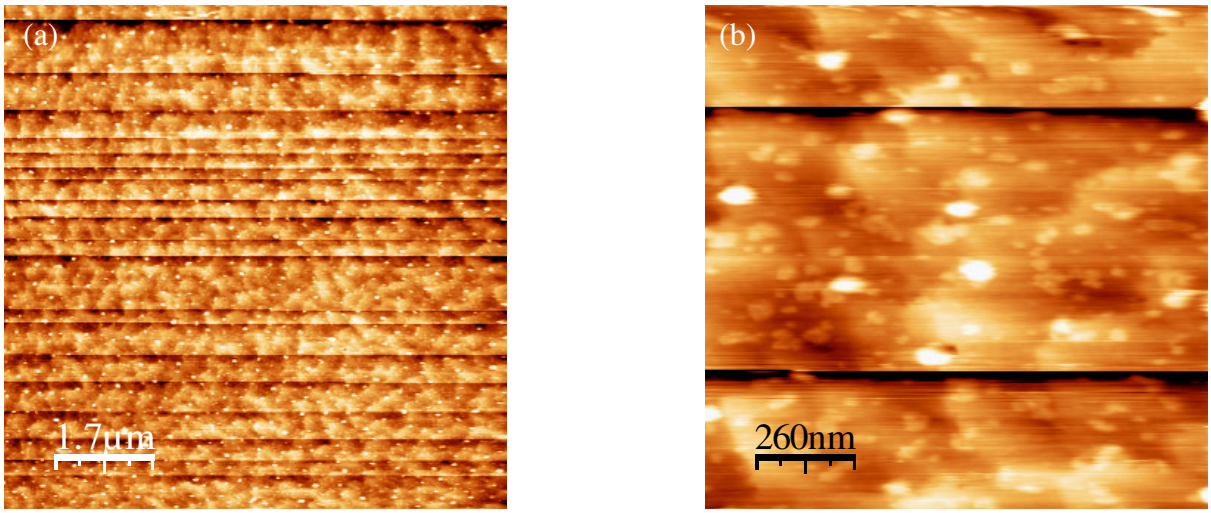

Figure 4.4 : Atomic Force Micrographs of LSMO on 2 degree stepped STO substrates 25nm thin film. The steps are very clear in the figures a-c and roughness of the film is 2.59666 (d).

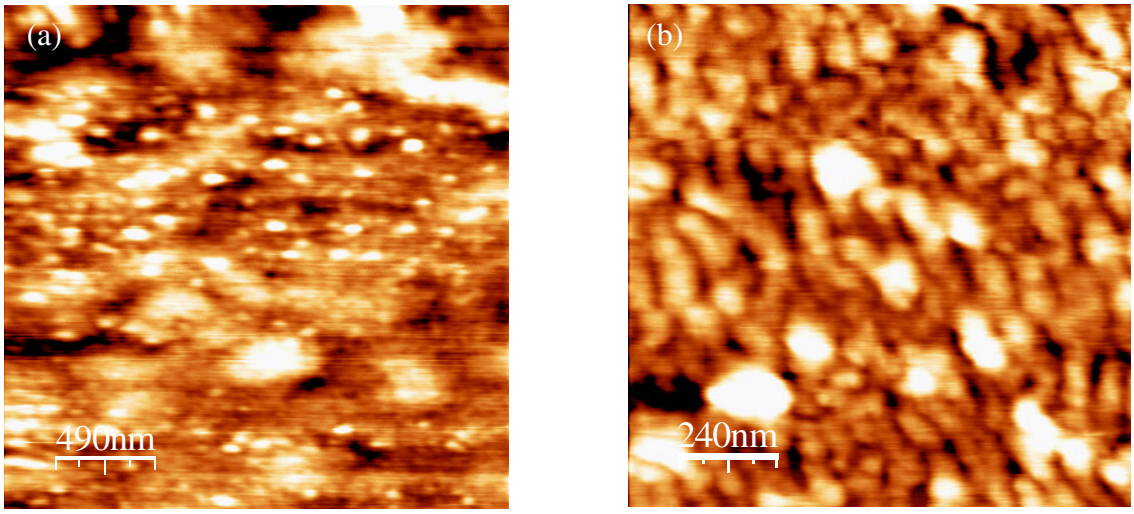

Figure 4.5: AFM micrographs of LSMO/LAO (a) and LSMO/NGO (b) reveals that grain density if higher for LAO due to compressive stress as compared to NGO substrates, which is comparatively relaxed substrate for LSMO.

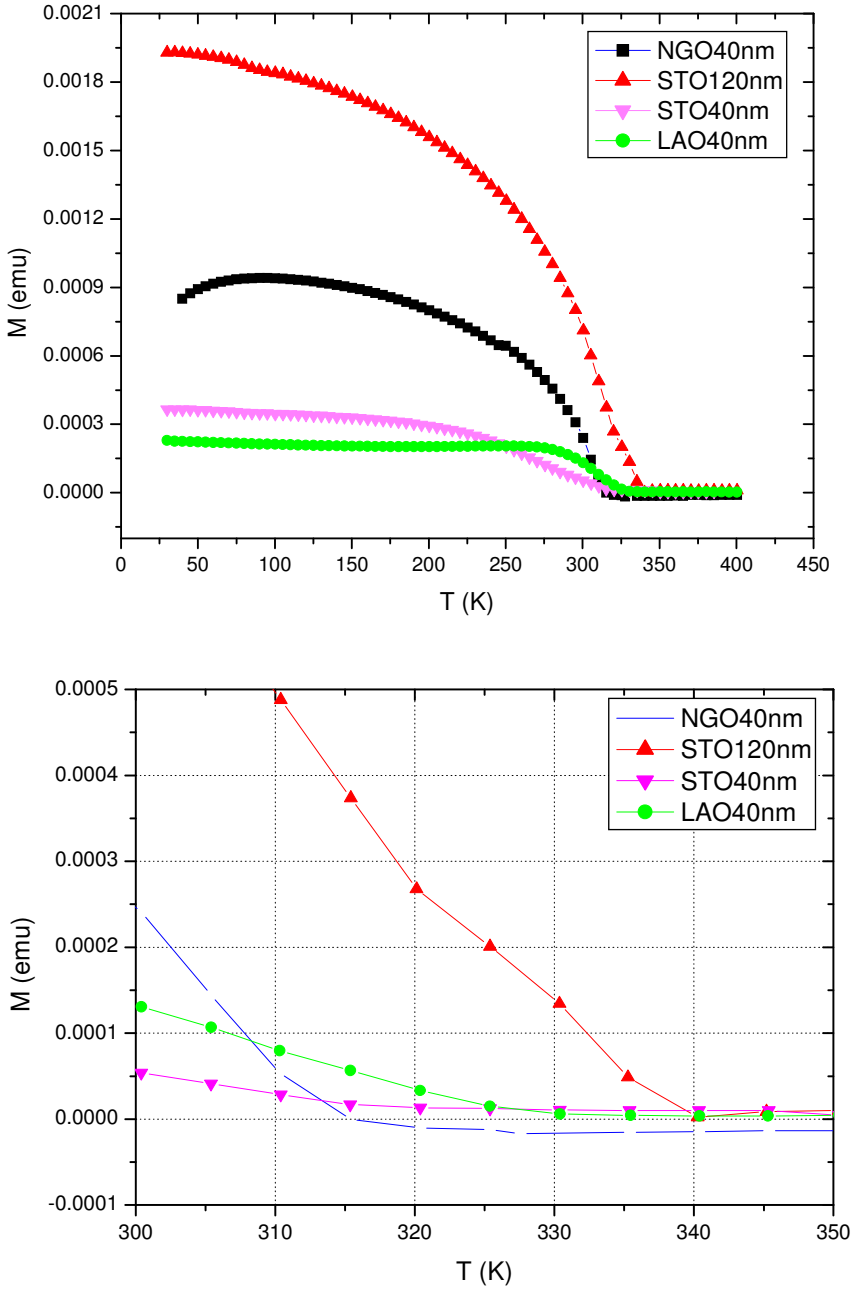

Figure 4.6: Magnetization versus Temperature for four LSMO thin on SOT (40&120nm), on LAO (40nm) and NGO (40nm). B is the enlarge graph near the ferromagnetic transition temperature. It is clear the Curie temperature for LSMO thin films is independent to substrate but dependent on thickness of thin films.

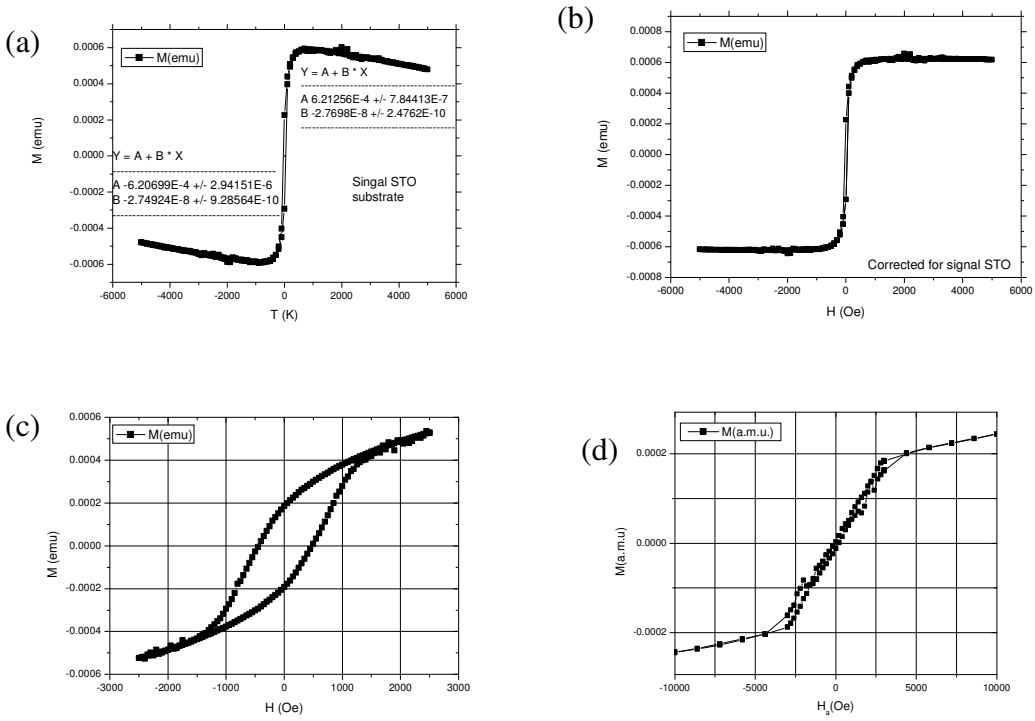

Figure 4.7: Magnetization versus applied magnetic field curves for LSMO on STO in plane (a), corrected for substrate signal (b), LSMO on ALO in Plane (c), out of plane (d).

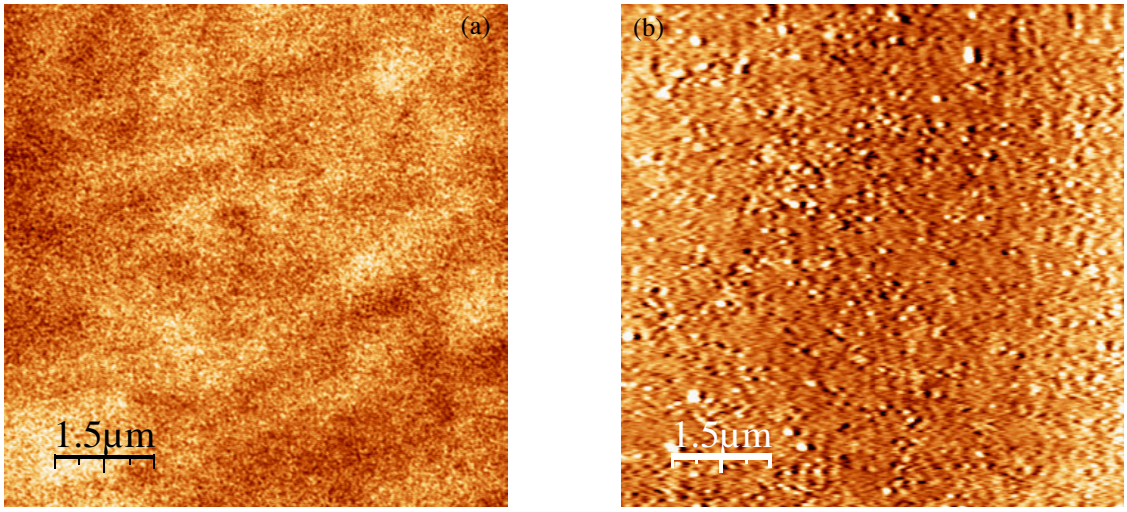

Figure 4.8: Magnetic Force Micrograph of LSMO/STO thin film (20nm) over 7.5µm ×7.5µm scan (a) shows weak magnetic contrast due to in plane magnetization. If domain wall are Block wall (Wall for which magnetic moments rotate in semi circular form from one direction to other) then image should be very clear but in case of Neel Wall (Walls for which magnetic moments rotate in a plan form one direction to other) then there will be no any contrast. In this MFM Image contrst is very weak it means that there are both kind of wall but dominate are Neel walls. (b) Topographical view.

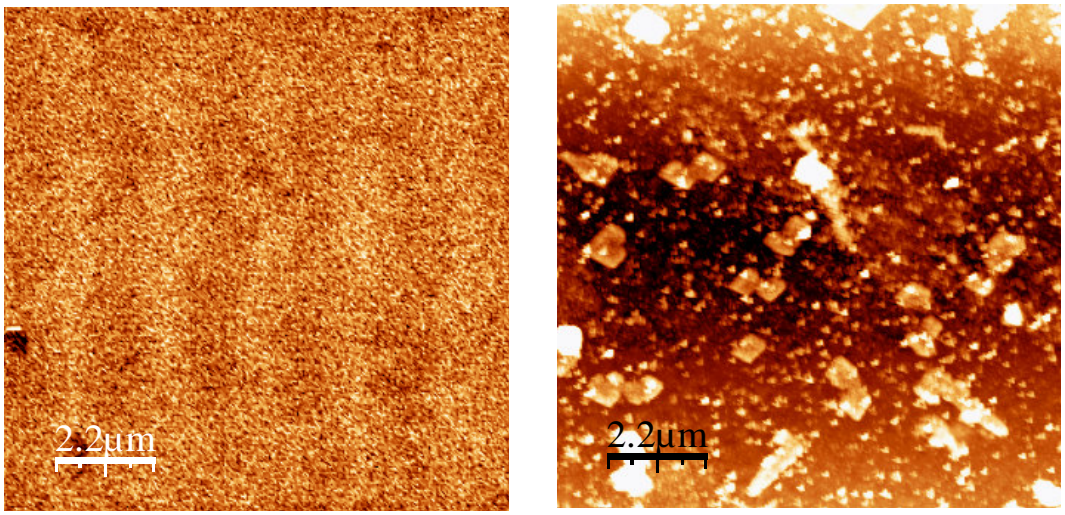

Figure 4.9: Magnetic Force Micrograph of LSMO/STO thin film (40nm) weak strip like magnetic contrast, magnetization is in-plane while magnetic image is being clear due to increase in thickness of thin film (left) Topographical view (right).

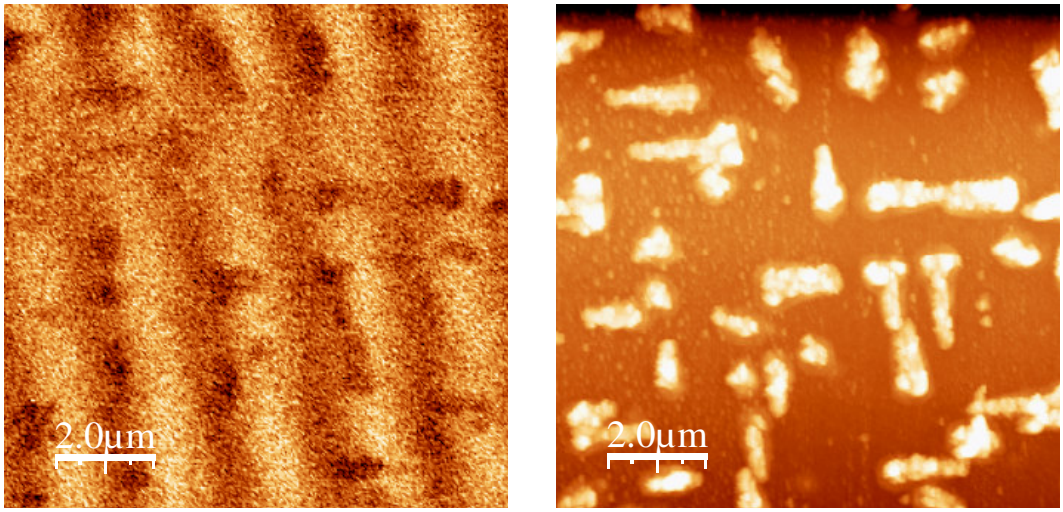

Figure 4.10: Magnetic Force Micrograph of LSMO/STO thin film (120nm) clear strip magnetic domains due to thick films that induced relaxation in the films (left). The spacing between neighbouring domains is about 1.15 µm. Topographical view (right).

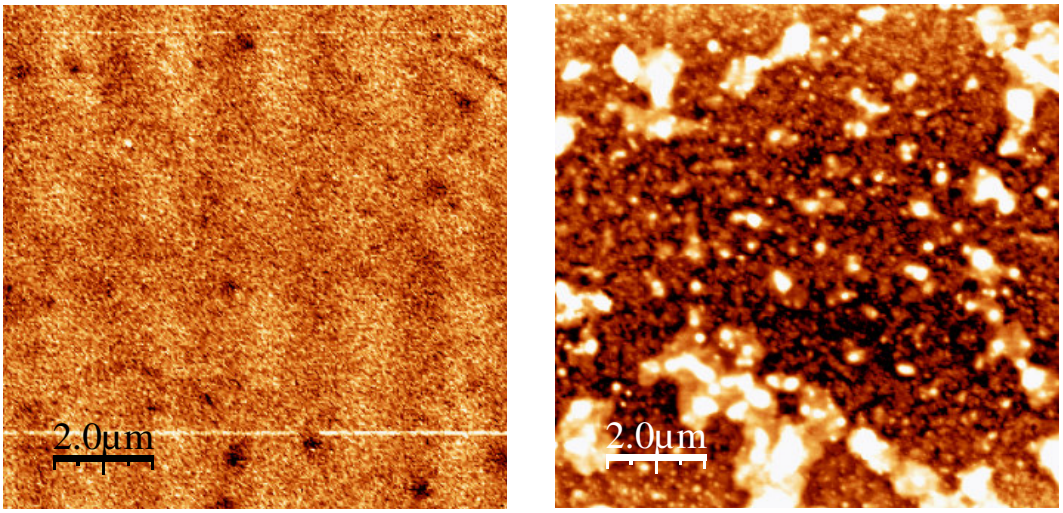

Figure 4.11: Magnetic Force Micrograph of LSMO thin film on 2° stepped STO substrate (25nm) over 10µm ×10µm scan. Magnetic microstructure is more clear that LSMO/STO with 40 nm thickness because of relaxation in film by steppes on substrate (left) Topographical view (right).

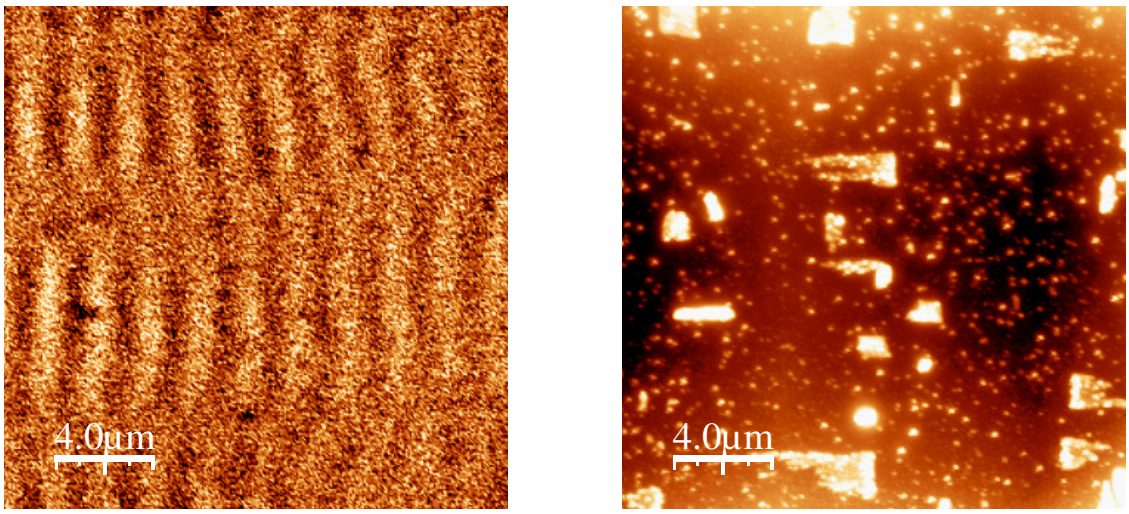

Figure 4.12: Magnetic Force Micrograph of LSMO/LAO thin film (40nm) over 20µm ×20µm scan (a) strip like magnetic contrast due to out of plane magnetization (b) Topographical view. The spacing between neighbouring domains is about 1.13 µm.

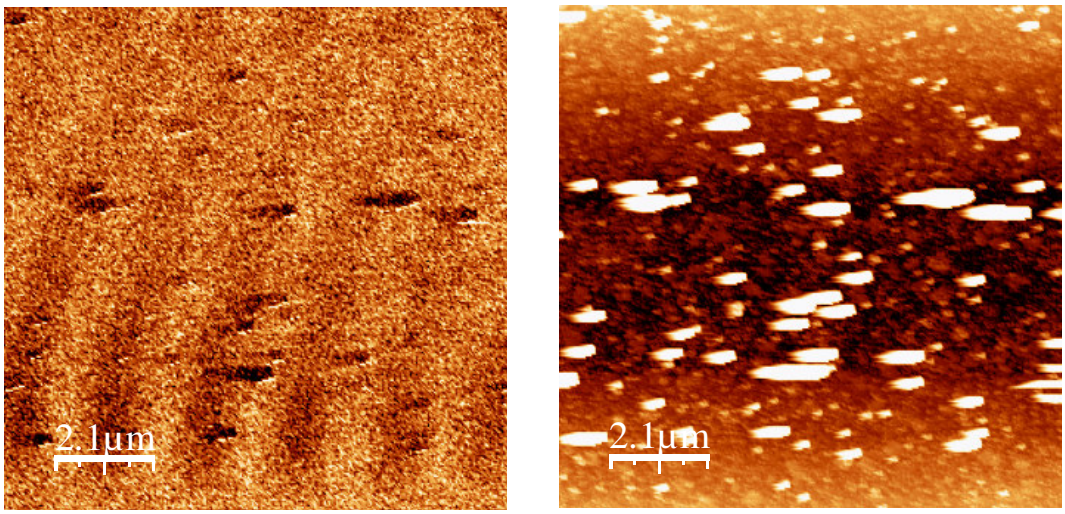

Figure 4.13: Magnetic Force Micrograph of LSMO/NGO thin film (40nm) over 10.5µm ×10.5µm scan. There are also signatures of big grains in the magnetic image on left due to contact of MFM tip with grains during scan in lift mode. Topographical view is on right side.

Table 4.1: Lattice parameters of LSMO thin films and of various substrates along with lattice mismatch and distortion

Substrate / film thickness	Substrate Parameter (Å)	Film Parameters (Å)	Mismatch	Distortion
STO/20nm	a = 3.9050	a = 3.8925 c = 3.8527	0.3201	1.0103
STO/40nm	a = 3.9051	a = 3.9046 c = 3.8537	0.0128	1.0132
STO/120nm	a = 3.9055	a = 3.9029 c = 3.8539	0.0666	1.0127
NGO/40nm	a = 3.8573	a = 3.9075 c = --------	-1.3014	~1
LAO/40nm	a = 3.7896	a = 3.8338 c = 3.9491	-1.1663	0.9708

Table 4.2: Curie temperature and Coercive fields of LSMO thin films on various substrates of different thickness.

Substrate	Thickness (nm)	T_c (K)	Coercive Field (Oe) (In-Plan)	Coercive Field (Oe) (Out of Plane)
NGO	40	316	----	
LAO	40	336	450	
STO	40	321	36	
STO	120	341	26	

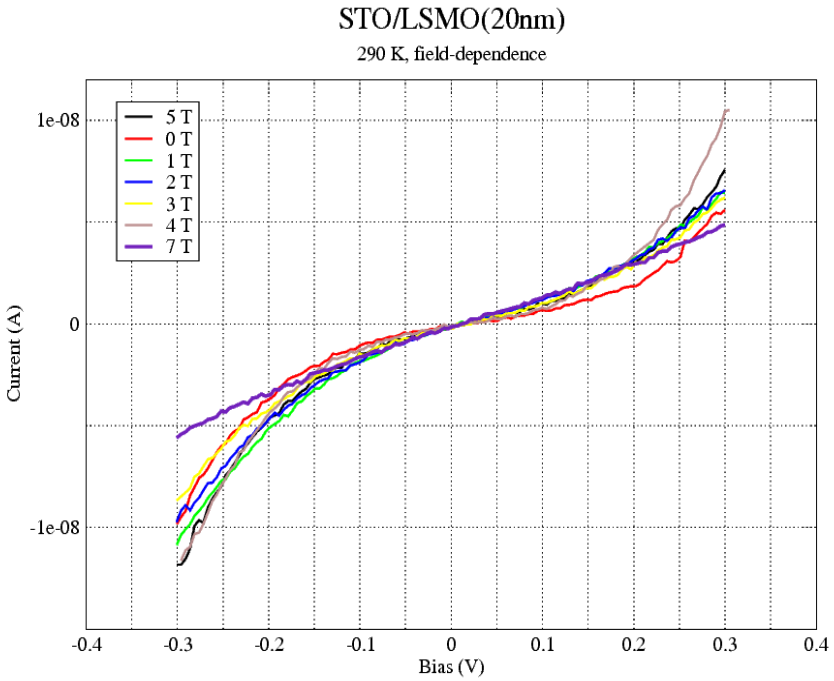

Figure 4.14: Current versus Voltage behavior of LSMO/STO thin film (20nm) at 290K and varied magnetic field analyzed by STM. The curve for 7T is more like metal behavior. For other values of magnetic field it is quite similar to each other.

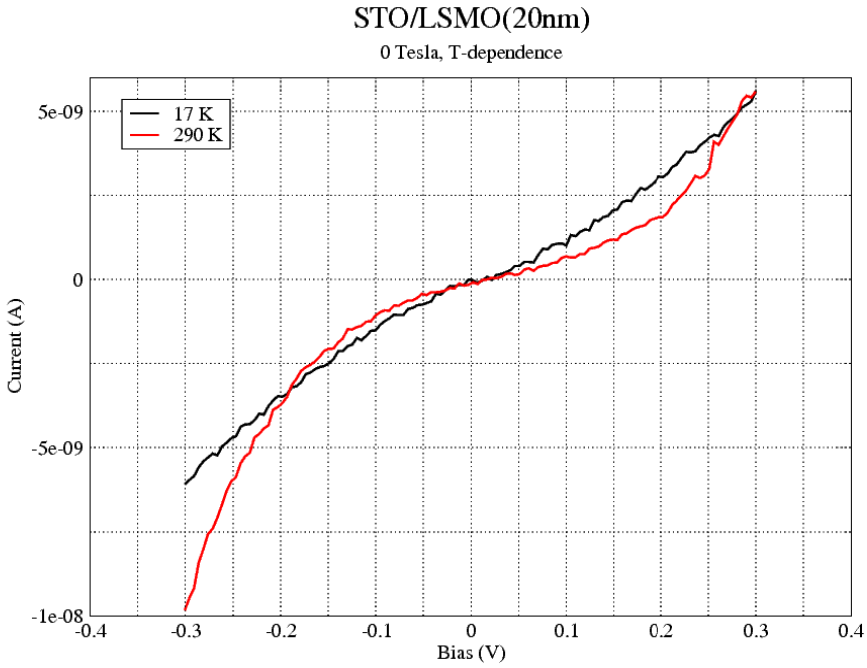

Figure 4.15: Current versus Voltage behavior of LSMO/STO thin film (20nm) at zero applied magnetic field analyzed by STM. The curve for 17K shows more better metal behavior as compared to 290K, which indicate semiconductor like behavior because the curie temperature of LSMO is 350K where is it Insulator.

Chapter 5

Conclusions

Feather like magnetic domains have been observed in 20nm $La_{0.67}Sr_{0.33}MnO_3$ thin films on normal (100) STO substrate due to in plane magnetization induced by tensile stress and presence of both Block and Neel walls. These magnetic domains were transformed into straight strip like magnetic domains by increasing the thickness of thin films up 120nm with domain separation of 1.15μm. It was also investigated that 25nm LSMO thin films on 2° stepped STO substrate have also strip like magnetic domains due to relation induced by stepped substrate. Magnetic microstructures were again straight strips with separation of about 1.13μm in LSMO thin films under compressive stress on LAO and NGO. The magnetization vector was out of plane for LSMO/LAO 40nm think films.

The ferromagnetic transition temperature Tc was also measured for LSMO on STO, LAO and NGO substrates. It was found that Curie temperature for LSMO thin films has no dependence on underlying substrate but strongly dependent on thickness of thin film.

References

1. J. G. Bendnorz and K. A. Muller Z. Physik B, **64** 189 (1986).
2. S. Jin, T. H. Tiefel, M. McCormack, R. A. Fastnacht, R. Ramesh and L. H. Chen, Science **264** 413 (1994).
3. H. Y. Hwang, S. W. Cheong, P. G. Radaelli, M. Marezio and B. Battogg, Phys. Rev. Lett. **75** 914 (1995).
4. J. Dho, W. S. Kim and N. H. Hur, Phys. Rev. Lett. **89** 027202 (2002).
5. R. von Helmelt J. Wecker, B. Holzapfel, L. Schultz, and K. Samwer, Phys. Rev. Lett. **71** 2331 (1993).
6. J. B. Goodenough, J. Applied Phys. **81** 5330 (1997).
7. W. Prellier, Ph. Lecoeur, and B. Mercey, J. Phys.: Condens. Matter **13**, R915 (2001).
8. C. Kwon, M. C. Robson, K.-C. Kim, J. Y. Gu, S. E. Lofland, S. M. Bhagat, Z. Trajanovic, M. Rajeswari, T. Venkatesan, A. R. Kratz, R. D. Gomez, and R. Ramesh, J. Magn. Magn. Mater. **172**, 403 (1997).
9. H. S. Wang and Q. Li, Appl. Phys. Lett. **73**, 2360 (1998).
10. J. Z. Sun, D.W. Abraham, R. A. Rao, and C. B. Eom, Appl. Phys. Lett. **74**, 3017 (1999).
11. R. Desfeux, S. Baileul, A. Da Costa, W. Prellier, and A. M. Haghiri-Gosnet, Appl. Phys. Lett. **78**, 3681 (2001).
12. Y. Wu, Y. Suzuki, U. Ru¨diger, J. Yu, A. D. Kent, T. K. Nath, and C. B.Eom, Appl. Phys. Lett. **75**, 2295 (1999).
13. Y. Wu, Y. Matsushita, and Y. Suzuki, Phys. Rev. B **64**, 220404 (2001).
14. Y. Suzuki, H. Y. Hwang, S.-W. Cheong, and R. B. van Dover, Appl. Phys. Lett. **71**, 140 (1997).
15. Q. Lu, C.-C. Chen, and A. de Lozanne, Science **276**, 2006 (1997).
16. P. Lecoeur, P. L. Trouilloud, G. Xiao, A. Gupta, G. Q. Gong, and X. W. Li, J. Appl. Phys. **82**, 3934 (1997).
17. C. H. Marrows, Advances in Physics, **54** 585 (2005).
18. P. Weiss, J. Physique Radium, **6** 661 (1907).
19. P. Weiss and G. Foes, Le Magnetism (Armand Colln, Paris, 1926).
20. C. Kittle, Rev. Mod. Phys. **21** 541 (1932).
21. L. D. Landau and E. Lifschitz, Phys. Z. Sowjetunion **8** 153 (1935).

22. F. Bloch, Z. Phys. **74** 295 (1932).
23. D. Spisák and J. Hafner, *Phys. Rev. B*, **55**, 8304 (1997).
24. D. Spisák and J. Hafner, *J. Magn. Magn. Mat.*, **168** 257 (1997).
25. Z. Q. Yang, R. W. A. Hendrikx, J. Aarts, Y. Qin, and H. W. Zandbergen, Phys. Rev. B **67,** 024408 (2003).